Low-loss and Thermal-stable Ta_2O_5 Photonic Platform with Low-temperature Process

Zhaoting Geng[1], Weiren Cheng[1], Zhenyu Liu[1], Mingjian You[1], Xiaolun Yu[1], Pengzhuo Wu[1], Ning Ding[1], Xingyu Tang[1], Yihan Liu[1], Li Shen[2], and Qiancheng Zhao[1*]

[1]*School of Microelectronics, MOE Engineering Research Center of Integrated Circuits for Next Generation Communications, Southern University of Science and Technology, Shenzhen, Guangdong, 518000, China*

[2]*Wuhan National Laboratory for Optoelectronics, Huazhong University of Science and Technology, 430074 Wuhan, China*

**zhaoqc@sustech.edu.cn*

Abstract: We demonstrate a Ta_2O_5 photonic platform with a propagation loss of 0.5dB/cm and a thermo-optic coefficient of 2.3×10^{-6} /K at 1550 nm. The process temperature is below 350℃, friendly to integration with other optoelectronic components.

1. Introduction

Integrating low-loss photonic platforms with active materials such as lithium niobate [1], III-V compound semiconductors [2], and phase change materials [3], equips passive lightwave circuits with unprecedented functionalities. However, the monolithic integration of optoelectronic and passive photonic components is hindered by the high-temperature processes that are often required in low-loss photonic platforms. For example, ultra-low-loss Si_3N_4 photonic platforms [4,5] rely on annealing processes that are over 1050 ℃, which restricts these platforms to be used in the front-end-of-line processes only. Thus, it is necessary to search for alternative photonic platforms that can be fabricated at low temperature with comparable technical performance. In recent years, Ta_2O_5 emerged as a promising candidate material to address the problem. Progress has been achieved in developing low-loss Ta_2O_5 waveguides [6,7], but there lacks a systematic study of the loss origins in a wider spectral range, leaving little guidance to further improve the propagation loss performance.

In this work, we report a CMOS-compatible and low-loss Ta_2O_5 integrated photonic platform using a wafer-scale low-temperature process. We measure a loaded Q factor of 4.2×10^5 from a 2 mm-radius Ta_2O_5 micro-ring resonator at 1550 nm wavelength, corresponding to a propagation loss of 0.5 dB/cm. The thermo-optic coefficient of Ta_2O_5 is extracted to be 2.3×10^{-6} /K, 11 times smaller than that of the Si_3N_4. Thermal bistability measurement is performance in the entire C-band for the first time, to the best of the authors' knowledge. The results demonstrate the potential to reach even lower propagation loss down to 0.1 dB/cm.

2. Device Fabrication and Propagation Loss Characterization

A 90 nm-thick Ta_2O_5 film is deposited via ion beam sputtering on a 5 μm-thick thermal oxide substrate and patterned using contact lithography, and subsequently cladded with a 5 μm-thick 350 ℃ PECVD SiO_2 upper cladding. The waveguide core width is 2.8 μm to ensure the single TE mode operation at this thickness. The ring resonator has a radius of 2 mm with a ring-bus waveguide coupling gap of 1.25 μm. The transmission spectra of the resonator are measured by directly tuning the laser wavelength, and are fitted with Lorentzian curves to extract the loaded Q factors. Shown in Fig. 1(b), the free spectral range (FSR) around 1550 nm is 0.12 nm, corresponding to a group index of 1.595. The full width at half maximum (FWHM) of one resonance (Fig. 1(c)) is fitted to be $\Delta\lambda = 3.69$ pm, yielding a loaded Q factor to be $Q_l = \lambda_{res}/\Delta\lambda = 4.2 \times 10^5$. The propagation loss and the intrinsic Q factor are thus derived to be ~0.5 dB/cm and $Q_i = 5.7 \times 10^5$, respectively. The propagation loss and the loaded Q factor exhibit wavelength dependency as shown in Fig. 1(d). The propagation loss is above 1 dB/cm when the wavelength is shorter than 1500 nm, but decreases as the wavelength increases, and reaches down to 0.4 dB/cm at 1572 nm. The loaded Q factor shows the opposite trend as expected. The reason for the wavelength dependency is likely due to the material loss which will be examined and analyzed shortly.

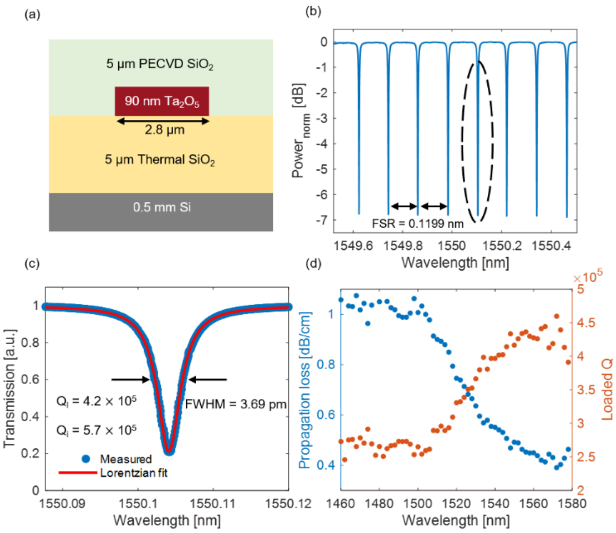

Fig. 1. (a) The waveguide cross-sectional geometry. (b) The transmission spectrum of a 2 mm-radius all-pass ring resonator in the spectral range from 1549.5 nm to 1550.5 nm reveals the TE mode operation only. (c) Lorentzian fit to the resonance circled in (b) shows a loaded Q factor of 4.2×10^5 and an intrinsic Q factor of 5.7×10^5. (d) The loaded Q factor and propagation loss as a function of wavelength in a range from 1460 nm to 1580 nm.

3. Thermal Response

The waveguide temperature sensitivity is characterized by tracking the resonant wavelength of the same azimuthal mode at different temperatures (Fig. 2(a)). The temperature dependent wavelength shift (TDWS) is measured to be $\beta = 9.69$ pm/K, which is a consequence of both the thermal expansion (TE) effect and the thermorefractive (TR) effect. The TDWS for the Ta_2O_5 resonator is smaller than the Si_3N_4 based resonant device [8]. Following the method in Ref. [9], we extract the thermo-optic coefficient of Ta_2O_5 to be 2.3×10^{-6} /K, which is nearly 11 times smaller than that of the Si_3N_4 [10].

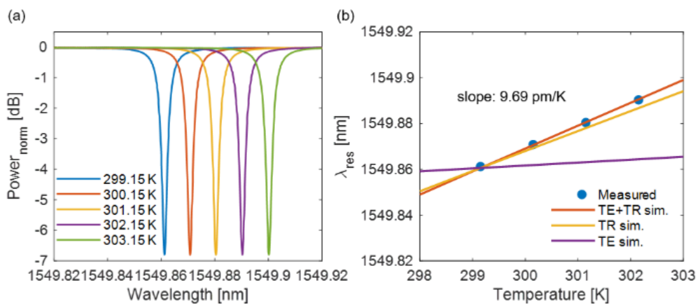

Fig. 2. (a) The temperature-dependent transmission spectrum of a 2 mm-radius ring resonator. (b) The simulated and measured center resonant wavelengths as a function of temperature.

4. Propagation Loss Analysis

To investigate the loss origins of the Ta_2O_5 waveguide, we performed a thermal bistability measurement [4,5,11] on this resonator, through which a linear relationship between the resonance frequency shift Δf_{res} and the on-chip power P_{in}, can be observed (Fig. 3(a)). The measured thermal susceptibility, defined as $\chi_{\mathrm{th}} = \Delta f_{\mathrm{res}}/P_{\mathrm{d}}$, is 23.27 MHz/mW, where $P_{\mathrm{d}} = P_{\mathrm{in}}(1 - T_{\mathrm{res}})$ is the dropped power, T_{res} is transmission at the resonance wavelength. The fraction of the absorbed power can be calculated as $\xi = \chi_{\mathrm{th}}/\beta R_{\mathrm{th}}$, where R_{th}=28.3 K/W is the thermal resistance which is obtained from a finite-element (FEM) simulator. With β equal to 1.1651 GHz/K, the fraction of the absorption power is estimated to be 70%, demonstrating that a significant amount of optical power is dissipated through material absorption. The propagation loss stemmed from material absorption and radiation (non-absorption) are plotted over a wavelength span from 1530 nm to 1570 nm. Shown in Fig. 3(b), the absorption-induced propagation loss gets reduced as the wavelength becomes longer. Substituting the current PECVD SiO_2 upper cladding by low-absorption SiO_2 materials, such as the sputtered SiO_2 [6] or the thermal oxide [12] may further reduce the total propagation loss down to 0.1 dB/cm.

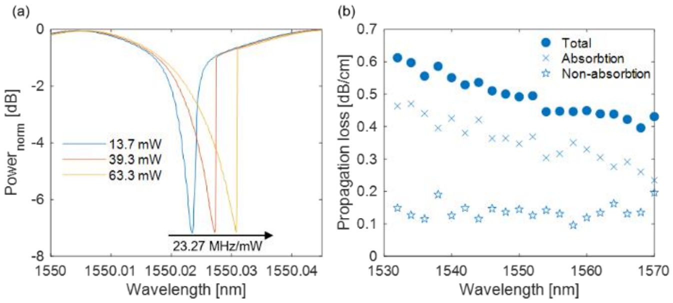

Fig. 3. (a) The skewed resonance measured under different power. The power indicated in the figure denotes the on-chip power. (b) Total and absorption propagation loss measurement from 1530 nm to 1570 nm for the resonator mentioned above.

In conclusion, we demonstrated a CMOS-compatible, low-loss and thermal-stable Ta_2O_5 integrated photonic platform using a low-temperature fabrication process without advanced lithographic tools or deuterated materials. The material absorption fraction of Ta_2O_5 waveguides is studied in the entire C-band for the first time, to the best of the authors' knowledge. The waveguide propagation loss could be reduced to 0.1 dB/cm by properly addressing the oxide cladding material absorption issue, demonstrating a great potential for power delivering and high-Q resonance applications.

Acknowledgment

This work is partially funded by National Natural Science Foundation of China (62205137), Basic and Applied Basic Research Foundation of Guangdong Province (2023A1515012141, 2021B1515120074), Wuhan National Laboratory for Optoelectronics (2021WNLOKF001). The authors acknowledge the assistance of SUSTech Core Research Facilities.

References

1. M. Churaev, R. N. Wang, A. Riedhauser, V. Snigirev, T. Blésin, C. Möhl, M. H. Anderson, A. Siddharth, Y. Popoff, U. Drechsler, D. Caimi, S. Hönl, J. Riemensberger, J. Liu, P. Seidler, and T. J. Kippenberg, Nat Commun **14**, 1 (2023).
2. C. Xiang, W. Jin, O. Terra, B. Dong, H. Wang, L. Wu, J. Guo, T. J. Morin, E. Hughes, J. Peters, Q.-X. Ji, A. Feshali, M. Paniccia, K. J. Vahala, and J. E. Bowers, Nature **620**, 78 (2023).
3. J. Geler-Kremer, F. Eltes, P. Stark, D. Stark, D. Caimi, H. Siegwart, B. Jan Offrein, J. Fompeyrine, and S. Abel, Nat. Photon. **16**, 491 (2022).
4. M. W. Puckett, K. Liu, N. Chauhan, Q. Zhao, N. Jin, H. Cheng, J. Wu, R. O. Behunin, P. T. Rakich, K. D. Nelson, and D. J. Blumenthal, Nat Commun **12**, 934 (2021).
5. M. H. P. Pfeiffer, J. Liu, A. S. Raja, T. Morais, B. Ghadiani, and T. J. Kippenberg, Optica **5**, 884 (2018).
6. M. Belt, M. L. Davenport, J. E. Bowers, and D. J. Blumenthal, Optica **4**, 532 (2017).
7. H. Jung, S.-P. Yu, D. R. Carlson, T. E. Drake, T. C. Briles, and S. B. Papp, Optica **8**, 811 (2021).
8. C. Xiang, W. Jin, J. Guo, J. D. Peters, M. J. Kennedy, J. Selvidge, P. A. Morton, and J. E. Bowers, Optica **7**, 20 (2020).
9. Q. Zhao, R. O. Behunin, P. T. Rakich, N. Chauhan, A. Isichenko, J. Wang, C. Hoyt, C. Fertig, M. hong Lin, and D. J. Blumenthal, APL Photonics **5**, 116103 (2020).
10. A. W. Elshaari, I. E. Zadeh, K. D. Jöns, and V. Zwiller, IEEE Photonics Journal **8**, (2016).
11. M. Gao, Q.-F. Yang, Q.-X. Ji, H. Wang, L. Wu, B. Shen, J. Liu, G. Huang, L. Chang, W. Xie, S.-P. Yu, S. B. Papp, J. E. Bowers, T. J. Kippenberg, and K. J. Vahala, Nat Commun **13**, 3323 (2022).
12. J. F. Bauters, M. J. R. Heck, D. D. John, J. S. Barton, C. M. Bruinink, A. Leinse, R. G. Heideman, D. J. Blumenthal, and J. E. Bowers, Opt. Express **19**, 24090 (2011).